CONF-880613--2

REDUCED-ACTIVATION AUSTENITIC STAINLESS STEELS: THE Fe-Mn-Cr-C SYSTEM*

CONF-880613--2

DE88 008091

R. L. Klueh and P. J. Maziasz

Metals and Ceramics Division, Oak Ridge National Laboratory

P.O. Box X, Oak Ridge, TN 37831-6376

ABSTRACT: Nickel-free manganese-stabilized stainless steels are being developed for fusion-reactor applications. As the first part of this effort, the austenite-stable region in the Fe-Mn-Cr-C system was determined. Results indicated that the Schaeffler diagram developed for Fe-Ni-Cr alloys cannot be used to predict the constituents expected for high-manganese steels. This is true because manganese is not as strong an austenite stabilizer relative to δ-ferrite formation as predicted by the diagram, but it is a stronger austenite stabilizer relative to martensite than predicted. Therefore, the austenite-stable region for Fe-Mn-Cr-C alloys occurs at lower chromium and higher combinations of manganese and carbon than predicted by the Schaeffler diagram. Development of a manganese-stabilized stainless steel should be possible in the composition range of 20 to 25% Mn, 10 to 15% Cr, and 0.1 to 0.25% C. Tensile behavior of an Fe-20%Mn-12%Cr-0.25%C alloy was determined. The strength and ductility of this possible base composition was comparable to type 316 stainless steel in both the solution-annealed and cold-worked condition.

KEY WORDS: manganese-stabilized stainless steels, reduced-activation steels, Fe-Mn-Cr-C alloys, Schaeffler diagram, austenite-stable alloys, martensite, δ-ferrite, tensile properties.

---

*Research sponsored by the Office of Fusion Energy, U.S. Department of Energy, under contract DE-AC05-84OR21400 with the Martin Marietta Energy Systems, Inc.

Austenitic stainless steels such as type 316 are being considered for use as structural materials in the first wall and blanket structure of magnetic fusion reactors. However, irradiation of alloys that contain Ni, Mo, Nb, N, or Cu in a fusion environment will produce long-lived radioactive isotopes, which lead to difficult radioactive waste-disposal problems when the structure is removed from service [1]. Such problems can be reduced by developing steels that contain only elements that produce radioactive isotopes that decay to low levels in a reasonable time.

A program is in progress to develop fast induced-radioactivity decay (FIRD) austenitic stainless steels to replace nickel-based stainless steels presently being considered for fusion reactor applications. For FIRD austenitic alloys, manganese was proposed as a replacement for nickel [2]. However, it was recognized that manganese is not as strong an austenite stabilizer as nickel, and it is not possible to simply replace nickel in Ni-Cr stainless steels with equal amounts of manganese. Therefore, an effort was made to first determine Fe-Mn-Cr-C compositions that produce a single-phase austenite microstructure, after which this base could be modified for strength and irradiation resistance.

As a first attempt to determine alloy compositions to use as a base composition, available phase diagrams and the Schaeffler diagram (Fig. 1) were consulted [3]. For the Schaeffler diagram, nickel and chromium equivalents were calculated according to the following relationships [3]:

$$\text{Ni Equiv} = (\text{Ni}) + (\text{Co}) + 0.5(\text{Mn}) + 0.3(\text{Cu}) + 25(\text{N}) + 30(\text{C}) \quad ; \quad (1)$$

$$\text{Cr Equiv} = (\text{Cr}) + 2(\text{Si}) + 1.5(\text{Mo}) + 5(\text{V}) + 5.5(\text{Al}) + 1.75(\text{Nb}) + 1.5(\text{Ti}) + 0.75(\text{W}), \quad (2)$$

where the concentration of the respective elements given in parentheses is in weight percent.

In this paper the results of those studies to determine a base composition will be examined. The tensile behavior of a possible base composition will be compared to the strength of type 316 stainless steel.

Experimental Procedure

Fifteen 600-g button heats of Fe-Mn-Cr-C were melted and cast (designated as PCMA-0 through PCMA-14) with compositions given in Table 1. Nominal compositions were chosen to locate boundaries of the austenite region with other phase or constituent regions of the Schaeffler diagram.

All of the alloys were cast into a rectangular cross section of 12.7 by 25.4 by 152 mm. The first ten alloy ingots were cold rolled to 6.4 mm in 30 to 50% increments of reduction, with homogenization treatments of 24 h at 1275°C applied after the cold-rolling reduction. Several of the steels were much more difficult to cold work than normal nickel-stabilized stainless steels, because they transformed to martensite during rolling and cracked badly. Because of the difficulties in cold rolling the first ten alloys, the last five were hot rolled at 1050°C. All of the heats except PCMA-3 were rolled to 0.76- and 0.25-mm-thick sheet; PCMA-3 cracked extensively when rolled.

Difficulties with rolling were also experienced with PCMA-5. The final sheet was in the 20% cold-worked condition.

Metallography and magnetic measurements were conducted on pieces of the homogenized material, pieces of the 20% cold-worked material, and on pieces of the cold-worked material that were annealed for 1 h at 1150°C and for 8 h at 1050°C. Magnetic measurements were made with a "Ferritescope" to obtain a qualitative measure of the ferromagnetic permeability of each alloy. All specimens were examined by optical microscopy, and selected specimens were examined by transmission electron microscopy (TEM).

In addition to the button melts, we obtained small amounts of 0.25-mm-thick sheet from a series of Fe-Mn and Fe-Mn-Cr steels from the Hanford Engineering Development Laboratory (HEDL), Richland, Washington. These had been produced as small button melts with the nominal compositions given in Table 2 [4]. Four of these specimens for which sufficient material was available were analyzed and found to have compositions sufficiently near the nominal Fe-Mn-Cr composition (but with some amounts of silicon and nitrogen) so that there was little difference when the nominal composition was assumed for calculating chromium and nickel equivalents. The small pieces of sheet were annealed 8 h at 1050°C before examination.

After the composition range of austenite stability was determined by microstructural studies, a small button melt of a potential base alloy composition was prepared. The ingot was reduced to 20% cold-worked 0.76-mm-thick sheet, using the procedures described above. Tensile tests at temperatures between room temperature and 600°C were

made on specimens in the cold-worked condition and after a solution anneal of 1 h at 1050°C. Specimens had a reduced gage section 20.3-mm long by 1.52-mm wide by 0.76-mm thick. All specimens were machined with gage lengths parallel to the rolling direction. Tests were made in vacuum on a 120-kN-capacity Instron universal testing machine at a crosshead speed of 8.5 μm/s, which results in a nominal strain rate of 4.2×10^{-4}/s.

Results and Discussion

Manganese as an Austenite Stabilizer

The microstructures of the fifteen Fe-Mn-Cr-C alloys were examined by optical microscopy after the homogenization treatment (24 h at 1275°C) and after the solution-anneal treatments of 1 h at 1150°C and 8 h at 1050°C; selected specimens were also examined by TEM. Based on the observations on solution-annealed steel together with the chemical compositions (Tables 1 and 2), magnetic measurements, phase diagrams, and the Schaeffler diagram, the microstructural constituents were identified. Detailed descriptions of the microstructural studies and the magnetic measurements were previously presented [5].

Microstructures observed for PCMA-0 through PCMA-14 along with those predicted by the Schaeffler diagram are given in Table 3, and Fig. 2 shows examples of the different types of microstructures observed. Except for the relative amount of a given phase or constituent present, the microstructures after homogenization and after 8 h at 1050°C were generally similar to those observed after 1 h at 1150°C

(Table 3). Delta-ferrite (δ), austenite (γ), and martensite (M) were identified as constituents. No precipitate phases are identified in Table 3 beyond stating that precipitates were observed, meaning that they were obvious by optical microscopy and distinguishable from δ, γ, or M. Possible precipitates could include carbides or Laves, sigma, and chi phases.

The most notable differences between the observed and predicted phases involved PCMA-0, -1, -5, -6, -9, -13, and -14. The major predicted constituents should have been either γ or γ + M, but the observations indicated that the major constituents were γ + σ.

Figure 3 shows the Schaeffler diagram with the compositions and constituents for the fifteen Fe-Mn-Cr-C alloys plotted on the diagram, using Eqs. (1) and (2) to calculate the chromium and nickel equivalents. It is clear that the diagram does not adequately describe the behavior of the high-manganese steels. In particular, the observed γ + δ field is considerably wider than predicted by the Schaeffler diagram [3]. Therefore, manganese does not appear to be as strong an austenite stabilizer against δ-ferrite formation as it would be if it were simply half as effective as nickel [as assumed in Eq. (1)]. The appearance of austenite and martensite also occurs at different compositions from those predicted by the Schaeffler diagram. In this case, manganese is a more potent austenite stabilizer against martensite than is accounted for by the simple nickel equivalency relationship.

To further delineate the differences between the Schaeffler diagram boundaries and the constituents in Fe-Mn-Cr-C alloys, we examined the eighteen Fe-Mn and Fe-Mn-Cr steels listed in Table 2. Again,

optical and electron microscopy observations were made [5], and the results are shown in Fig. 4, where the Schaeffler diagram is shown with the constituents of the alloys superimposed. Microstructures of many of these alloys also did not behave as predicted by the diagram. However, the differences generally agreed with the observations made on the Fe-Mn-Cr-C alloys.

Figure 5 shows a conventional Schaeffler diagram with all of the 33 alloys examined. In Fig. 6(a), a new, modified diagram is presented with boundaries redrawn so as to accommodate the microstructural observations. (Note that the $\gamma + \delta/\delta$ boundary was not determined and is estimated.) With a few exceptions near boundaries, the observations agree with the various regions as redrawn. Figure 6(b) shows the modified diagram superimposed on the conventional Schaeffler diagram.

The study showed that manganese is not as strong an austenite stabilizer relative to δ-ferrite as predicted by the Schaeffler diagram. Further, it is a stronger stabilizer of the austenite against the martensite transformation than predicted by the diagram. These results indicate that either the Schaeffler-diagram boundaries need to be altered for high-manganese alloys, or, alternatively, that the multiplying factor for manganese in Eq. (1) is not simply a constant of 0.5. Both approaches have been suggested [6-8].

Rather than search for an empirical relationship or relationships that will describe the behavior of manganese-scabilized stainless steels of the type being developed for fusion-reactor applications, we redrew the boundaries for austenite stability with chromium and nickel equivalents calculated by Eqs. (1) and (2). These boundaries delineate

the compositional region in which it should be possible to make austenite-stable alloys. Of course, these boundaries are estimates of the actual boundaries. More data would be required to firmly establish such boundaries. In Fig. 6, the boundaries are presented as straight lines, although there is no reason why they should not be curved [9].

It should be pointed out that the Schaeffler diagram was developed for weld or cast metal [3,9], and in this study it was applied to wrought material. Because inhomogeneities develop during solidification, the microstructure of annealed wrought material can differ considerably from that of weld metal or a casting. Annealed wrought material is closer to equilibrium than a cast material, and therefore, the $\gamma/\gamma + \delta$ boundary is shifted to the right – to higher chromium equivalents [10]. This is opposite to the change caused by manganese, further emphasizing the lower austenite-stabilizing capability of manganese. The closer approach to equilibrium of the annealed wrought steel will cause the $\gamma/\gamma + M$ boundary to be displaced downward parallel to the existing boundary (in the direction of lower nickel equivalents) [10]. This is in the same direction as the manganese effect. However, manganese has a much more pronounced influence on martensite formation, causing the apparent rotation of the boundary [Fig. 6(b)].

Since the ultimate objective of this study was the development of alloys that have properties equivalent to the austenitic stainless steels presently in the fusion-reactor materials program, it was decided to use Fig. 6 to reach that objective. Basically, the diagram

given in Fig. 6 shows that, to develop a manganese-stabilized austenitic stainless steel, it will be necessary to work with compositions that contain at least 20 to 25% Mn, 12 to 14% Cr, and 0.1 to 0.25% C.

Tensile Behavior of Base Composition

From the modified Schaeffler diagram, it was possible to pick a stable austenite composition for a manganese-stabilized stainless steel. As a first attempt to develop a suitable alloy, a base composition of Fe-20%Mn-12%Cr-0.25%C was chosen, and a steel of this nominal composition was melted, cast, fabricated, and tensile tested over the range room temperature to 600°C. The results were compared with type 316 stainless steel after both had received similar thermomechanical treatments.

The microstructures of the Fe-Mn-Cr-C alloy (labeled MnCrC) and type 316 stainless steel after both were solution annealed 1 h at 1050°C are shown in Fig. 7. Overall microstructures were quite similar, with both containing small precipitates throughout the cross section. Grain size for both steels were estimated as ASTM No. 4.

Figures 8 to 10 show a comparison of the tensile properties of type 316 stainless steel with the MnCrC in the solution-annealed and 20% cold-worked conditions (common conditions for using such a steel). The yield stress of the manganese-stabilized steel in both conditions was equivalent to that of the type 316 stainless steel (Fig. 8). Because of the higher work-hardening characteristics imparted by manganese, the MnCrC steel achieved a higher ultimate tensile strength for both thermomechanical conditions (Fig. 9). Despite this higher

work-hardening capability, the high-manganese steel still has equivalent or better ductility (as measured by total elongation) in the solution-annealed condition and equivalent ductility at all but 300 and 400°C in the cold-worked condition (Fig. 10). Even at 300 and 400°C in the cold-worked condition, the ductility remained adequate.

Future Work

Results discussed above indicate the range of manganese, chromium, and carbon compositions required to obtain a manganese-stabilized austenitic steel. Such a base composition must then be further alloyed to obtain the strength and resistance to irradiation-produced void swelling and helium embrittlement that will be necessary for fusion-reactor applications. In addition, the steel must be weldable and have compatibility with the coolant to which it will be subjected during service.

To obtain a steel with sufficient strength and irradiation resistance, methods used to obtain the U. S. austenitic prime candidate alloy (PCA) [11,12] will be applied (PCA is a Ni-Cr-Mo-Ti stainless steel). In PCA, void swelling is suppressed by the use of a high preirradiation dislocation density (cold work), which produces a high density of fine MC (titanium-rich) precipitates in the microstructure during irradiation [11,12]. Dislocations and fine precipitates retard swelling by acting as helium collection sites, giving rise to a high density of fine, stable cavities, which subsequently act as dominant sinks for the vacancies and interstitials produced during irradiation. The MC on grain boundaries in PCA imparts

resistance to helium embrittlement at elevated temperatures. Besides helping to control the helium and minimizing swelling, the MC strengthens the matrix by precipitation hardening [12].

We are presently investigating the effect of titanium on the strength of the base alloy discussed above. Phosphorous, boron, and vanadium additions will also be investigated. These elements are also used in some versions of PCA. PCA contains molybdenum, an element that must be eliminated in a FIRD steel. Tungsten is being investigated as a replacement for molybdenum.

Microstructural studies have been made on a series of Fe-20%Mn-12%Cr-0.25%C to which additions of Ti, W, V, B, and P have been made. Results indicate that it is possible to achieve microstructures comparable to those obtained in PCA [13]. Unirradiated tensile property studies on these alloys are in progress. Ultimately, the success of the alloys for fusion will have to be measured by their resistance to properties degradation during reactor irradiation. Selected tensile and TEM specimens are now being irradiated in the Fast Flux Test Facility and the High Flux Isotope Reactor.

Summary and Conclusions

The microstructures of a series of Fe-Mn-Cr-C and Fe-Mn-Cr alloys were examined to determine the constituents present in the solution-annealed condition. These observations were compared with expectations obtained using the Schaeffler diagram, which was developed primarily for Ni-Cr stainless steel weld metal with only small amounts of manganese. It was concluded that this diagram cannot be used to

predict the constituents expected for high-manganese steels. Manganese was found to be a weaker austenite stabilizer against δ-ferrite formation than predicted by the diagram, but it is a stronger austenite stabilizer against martensite than predicted. Therefore, for a manganese-stabilized stainless steel, the austenite-stable region is moved to lower chromium and relatively high combinations of manganese and carbon.

The objective of this work is the development of a manganese-stabilized austenitic stainless steel for fusion-reactor applications. It was concluded that an austenite-stable composition range that should allow for the development of such an alloy is 20 to 25% Mn, 12 to 14% Cr, and 0.1 to 0.25% C. Starting with such a base composition, it may be possible to alloy the steel for strength and irradiation resistance using the principles that were used to develop improved nickel-stabilized stainless steels for fusion-reactor applications. Tensile tests were conducted on an Fe-20%Mn-12%Cr-0.25% C steel – a possible base composition. Results indicated that the strength and ductility of this steel were similar to the strength of type 316 stainless steel in both the solution-annealed and cold-worked conditions.

Acknowledgements

We wish to thank F. A. Garner of HEDL for providing the Fe-Mn-Cr and Fe-Mn alloys. The help of the following people is gratefully acknowledged: T. K. Roche produced the button melts; L. T. Gibson and N. H. Rouse carried out the experimental tests and procedures; C. W. Houck did the optical metallography; J. F. King and M. L. Santella reviewed the manuscript; and Frances Scarboro typed the manuscript.

References

[1] R. W. Conn et al., "Panel Report on Low Activation Materials for Fusion Applications," UCLA Report PPG-728, University of California at Los Angeles, June 1983.

[2] R. L. Klueh and E. E. Bloom, *Optimizing Materials for Nuclear Applications*, F. A. Garner, D. S. Gelles, and F. W. Wiffen, Eds., The Metallurgical Society, Inc., Warrendale, Pennsylvania, 1985, pp. 73-85.

[3] H. Schneider, *Foundry Trade Journal*, Vol. 108, 1960, pp. 563-564.

[4] H. R. Brager, F. A. Garner, D. S. Gelles, and M. L. Hamilton, *Journal of Nuclear Materials*, Vol. 133&134, 1987, pp. 907-911.

[5] R. L. Klueh, P. J. Maziasz, and E. A. Lee, *Materials Science and Engineering*, to be published.

[6] E. R. Szumachowski and D. J. Kotecki, *Welding Journal*, Vol. 63, 1984, pp. 156s-163s.

[7] F. C. Hull, *Welding Journal*, Vol. 52, 1973, pp. 193s-203s.

[8] R. H. Espy, *Welding Journal*, Vol. 61, 1982, pp. 149s-156s.

[9] D. L. Olson, *Welding Journal*, Vol. 65, 1985, pp. 281s-295s.

[10] *Arcos Welding Products*, Arcos Corporation, Philadelphia, 1975, p. 29.

[11] P. J. Maziasz et al., *Journal of Nuclear Materials*, Vol. 108&109, 1982, pp. 296-298.

[12] P. J. Maziasz and T. K. Roche, *Journal of Nuclear Materials*, Vol. 103&104, 1981, pp. 797-802.

[13] P. J. Maziasz and R. L. Klueh, this volume.

Table 1. Chemical compositions of the Fe-Mn-Cr-C steel button heats

Alloy	Chemical composition,[a] (wt %)								
	C	Mn	Si	Ni	Cr	Mo	V	Cu	N
PCMA-0	0.069	13.4	0.04	0.01	15.0	0.01	0.01	0.03	0.001
-1	0.014	14.2	0.02	0.01	14.8	0.01	0.01	0.03	0.001
-2	0.056	17.1	0.04	0.01	15.2	0.01	<0.01	0.03	0.001
-3	0.089	13.9	0.02	0.01	10.0	0.01	<0.01	0.03	0.002
-4	0.093	18.9	0.02	0.01	9.9	<0.01	<0.01	0.02	0.002
-5	0.18	13.9	0.02	0.01	15.3	0.01	<0.01	0.04	0.002
-6	0.18	14.3	0.02	0.01	16.0	0.01	<0.01	0.03	0.003
-7	0.38	19.1	0.02	0.01	14.8	0.01	<0.01	0.05	0.005
-8	0.13	17.7	0.02	<0.01	20.1	0.01	<0.01	0.03	0.003
-9	0.26	17.6	0.03	0.01	20.2	0.01	<0.01	0.03	0.006
-10	0.081	19.9	0.04	0.01	10.0	0.01	0.01	0.02	0.005
-11	0.084	19.9	0.03	0.01	11.9	0.01	0.01	0.02	0.009
-12	0.18	20.0	0.02	0.01	12.0	0.01	0.01	0.02	0.008
-13	0.088	19.2	0.04	0.01	14.0	0.01	0.01	0.04	0.013
-14	0.17	19.9	0.05	0.01	15.9	0.01	0.01	0.02	0.001

[a]Balance iron.

Table 2. Chemical compositions of the Fe-Mn and Fe-Cr-Mn alloys

Nominal compositions

Fe–25Mn	Fe–5Cr–15Mn	Fe–10Cr–10Mn
Fe–30Mn	Fe–15Cr–15Mn	Fe–20Cr–20Mn
Fe–35Mn	Fe–10Cr–20Mn	Fe–20Cr–30Mn
Fe–40Mn	Fe–15Cr–20Mn	Fe–10Cr–40Mn
Fe–50Mn	Fe–5Cr–30Mn	Fe–5Cr–25Mn
	Fe–10Cr–30Mn	Fe–5Cr–35Mn
		Fe–10Cr–15Mn

Selected chemical analysis

Alloy	Chemical composition (wt.%)								
	C	Mn	Si	Ni	Cr	Mo	V	Cu	N
Fe–5Cr–15Mn	0.012	14.97	0.43	0.02	4.98	0.01	<0.01	0.03	0.008
Fe–10Cr–10Mn	0.013	11.28	0.19	0.01	9.75	0.01	<0.01	0.03	0.042
Fe–20Cr–30Mn	0.007	30.12	0.09	0.01	19.59	0.01	<0.01	0.03	0.006
Fe–10Cr–40Mn	0.021	39.35	0.38	0.02	9.81	0.01	<0.01	0.02	0.020

Table 3. Phases and constituents[a] predicted by Schaeffler diagram and those observed

Alloy	Phases and Constituents[b,c]	
	Predicted	Observed
PCMA-0	γ + M	γ + δ + M
-1	γ + M	γ + δ + M
-2	γ + M	γ + δ + M
-3	M	γ + M
-4	γ + M	γ + M
-5	γ + M	γ + δ
-6	γ	γ + δ
-7	γ	γ
-8	γ + δ	γ + δ
-9	γ	γ + δ
-10	γ + M	γ + M
-11	γ + M	γ
-12	γ	γ
-13	γ + M	γ + δ
-14	γ	γ + δ

[a]Identified by optical and transmission electron microscopy on steels annealed 1 h at 1150°C.

[b]γ = austenite, δ = δ-ferrite, and M = martensite.

[c]Precipitate phases are not listed because these are not given on Schaeffler diagram. Precipitate phases were observed by optical microscopy in PCMA-5, -6, -8, -9, and -10.

LIST OF FIGURES

Fig. 1. The Schaeffler diagram.

Fig. 2. Examples of the microstructures observed: (a) austenite (major phase) plus δ-ferrite (PCMA-6), (b) martensite (PCMA-3), and (c) austenite (PCMA-7). All specimens were annealed 1 h at 1150°C.

Fig. 3. Schaeffler diagram with the fifteen Fe-Cr-Mn-C alloys indicated; the phases observed for each alloy are shown.

Fig. 4. Schaeffler diagram with the eighteen Fe-Cr-Mn (some with 0% Cr) alloys indicated; the phases observed for each alloy are shown.

Fig. 5. Schaeffler diagram with the 33 experimental alloys indicated; phases observed for each alloy are shown.

Fig. 6. (a) A "modified Schaeffler diagram" with the phase boundaries redrawn in accordance with the observations for the high-manganese experimental alloys. (b) The modified diagram shown superimposed on the conventional Schaeffler diagram.

Fig. 7. Microstructures of (a) type 316 stainless steel and (b) an Fe-20%Mn-12%Cr-0.25%C alloy, both solution annealed 1 h at 1050°C.

Fig. 8. Yield stress behavior as a function of test temperature of type 316 stainless steel and an Fe-20%Mn-12%Cr-0.25%C alloy (MnCrC) after solution annealing 1 h at 1050°C and after 20% cold work.

Fig. 9. Ultimate tensile strength behavior as a function of test temperature of type 316 stainless steel and an Fe-20%Mn-12%Cr-0.25%C alloy (MnCrC) after solution annealing 1 h at 1050°C and after 20% cold work.

Fig. 10. Total elongation behavior as a function of test temperature of type 316 stainless steel and an Fe-20%Mn-12%Cr-0.25%C alloy (MnCrC) after solution annealing 1 h at 1050°C and after 20% cold work.

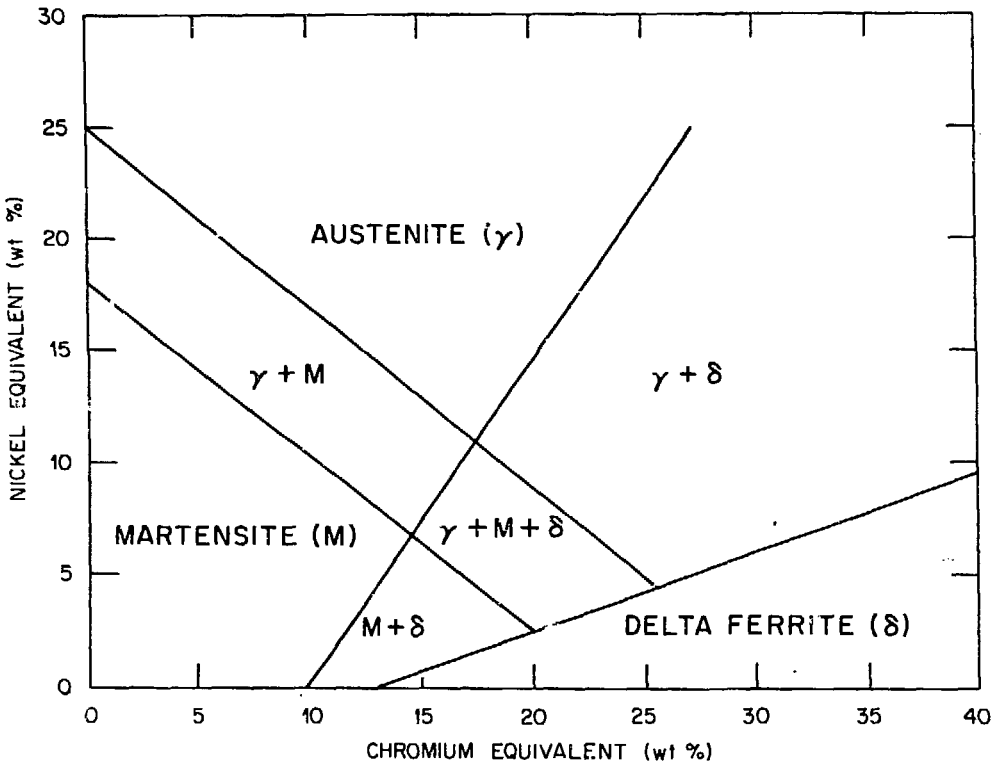

Fig. 1. The Schaeffler diagram.

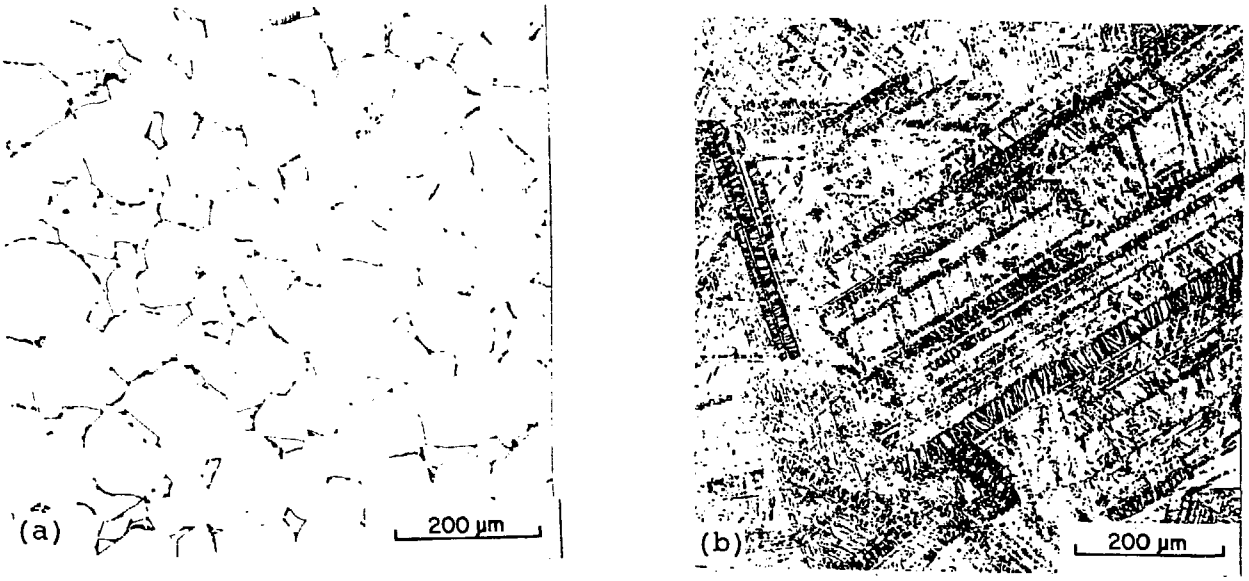

(c) 200 µm

Fig. 2. Examples of the microstructures observed: (a) austenite (major phase) plus δ-ferrite (PCMA-6), (b) martensite (PCMA-3), and (c) austenite (PCMA-7). All specimens were annealed 1 h at 1150°C.

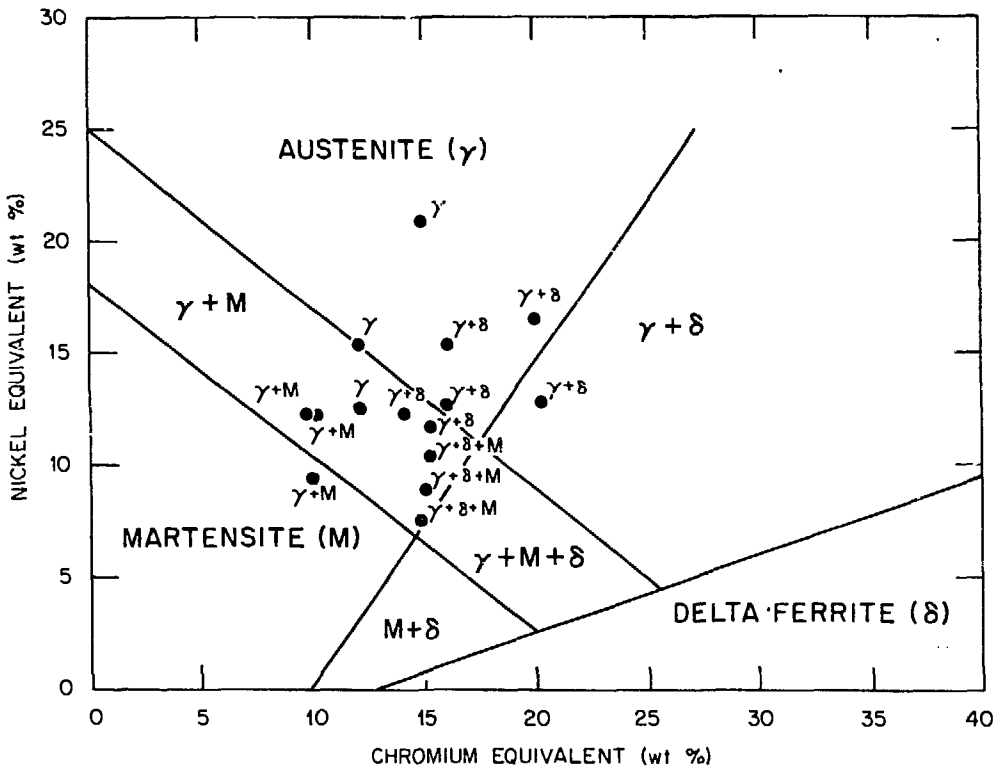

Fig. 3. Schaeffler diagram with the fifteen Fe-Cr-Mn-C alloys indicated; the phases observed for each alloy are shown.

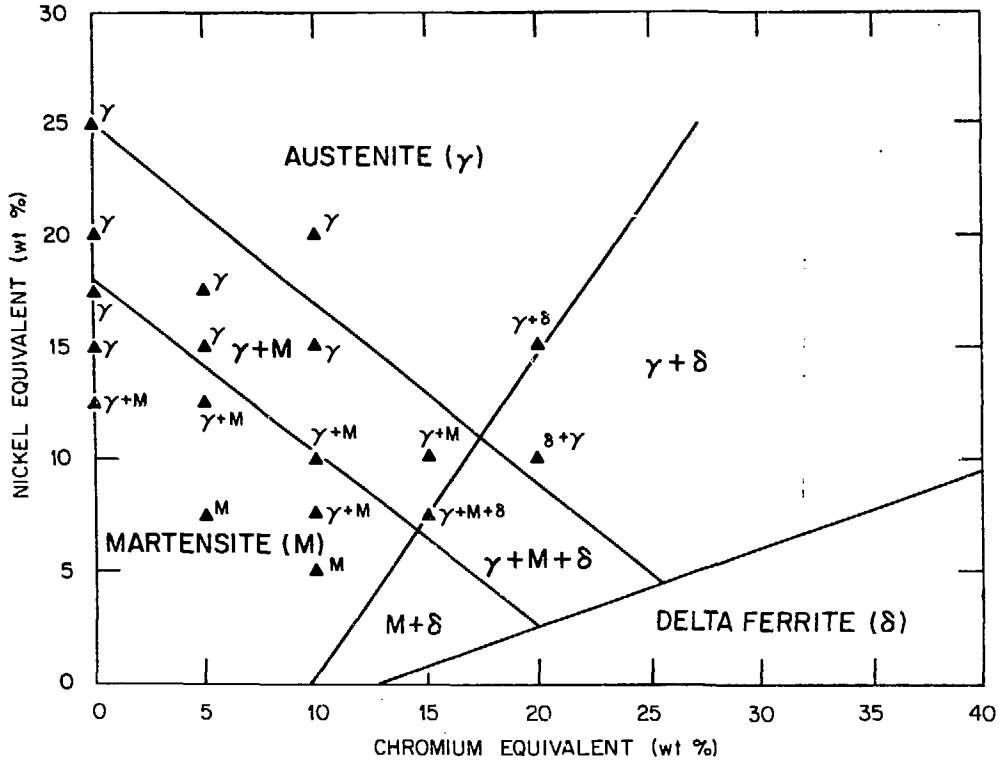

Fig. 4. Schaeffler diagram with the eighteen Fe-Cr-Mn (some with 0% Cr) alloys indicated; the phases observed for each alloy are shown.

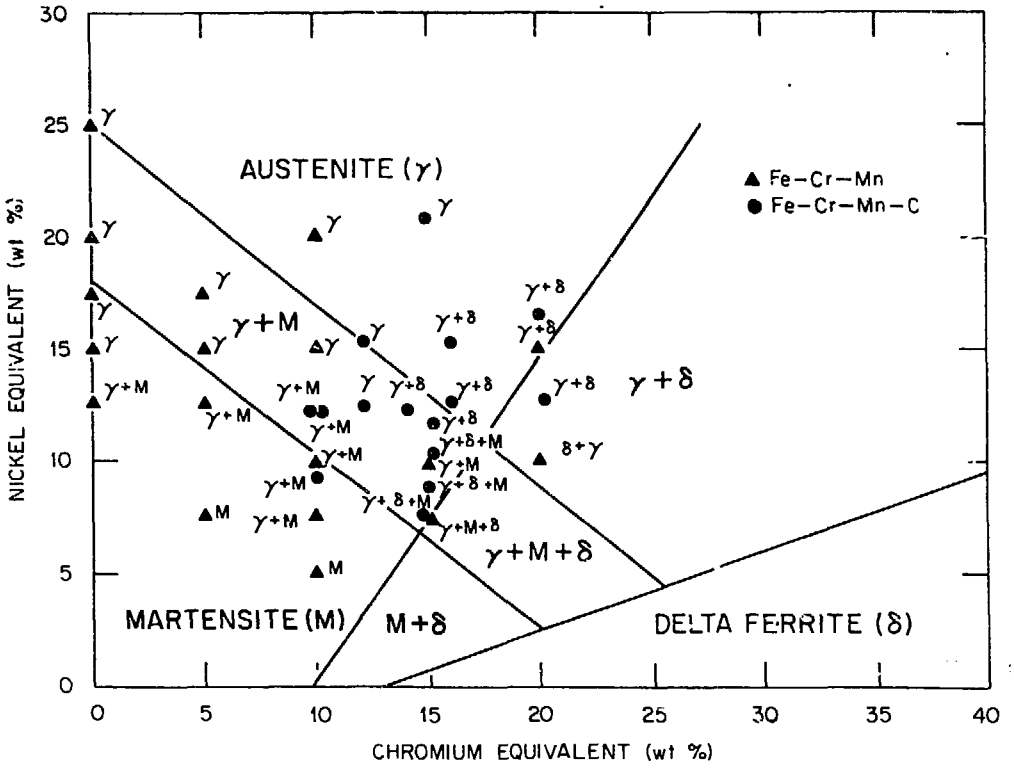

Fig. 5. Schaeffler diagram with the 33 experimental alloys indicated; phases observed for each alloy are shown.

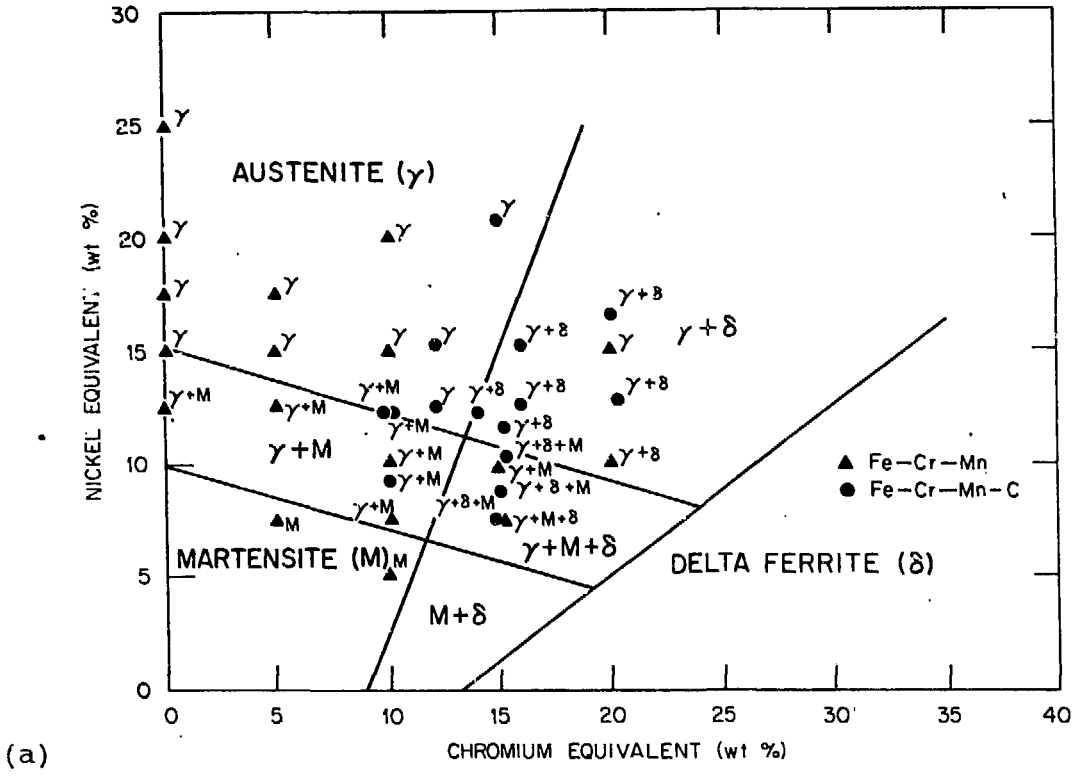

(a)

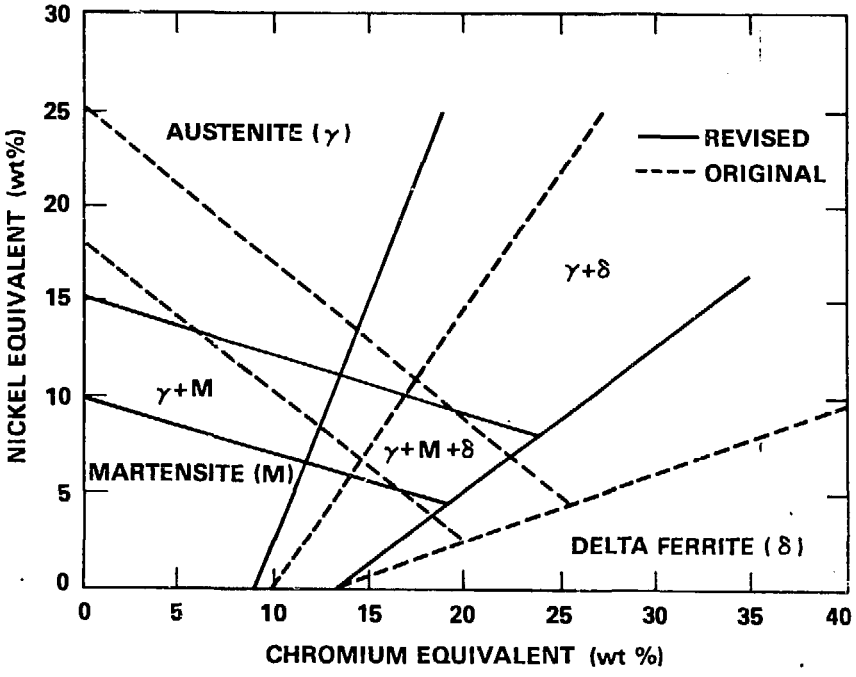

(b)

Fig. 6. (a) A "modified Schaeffler diagram" with the phase boundaries redrawn in accordance with the observations for the high-manganese experimental alloys. (b) The modified diagram shown superimposed on the conventional Schaeffler diagram.

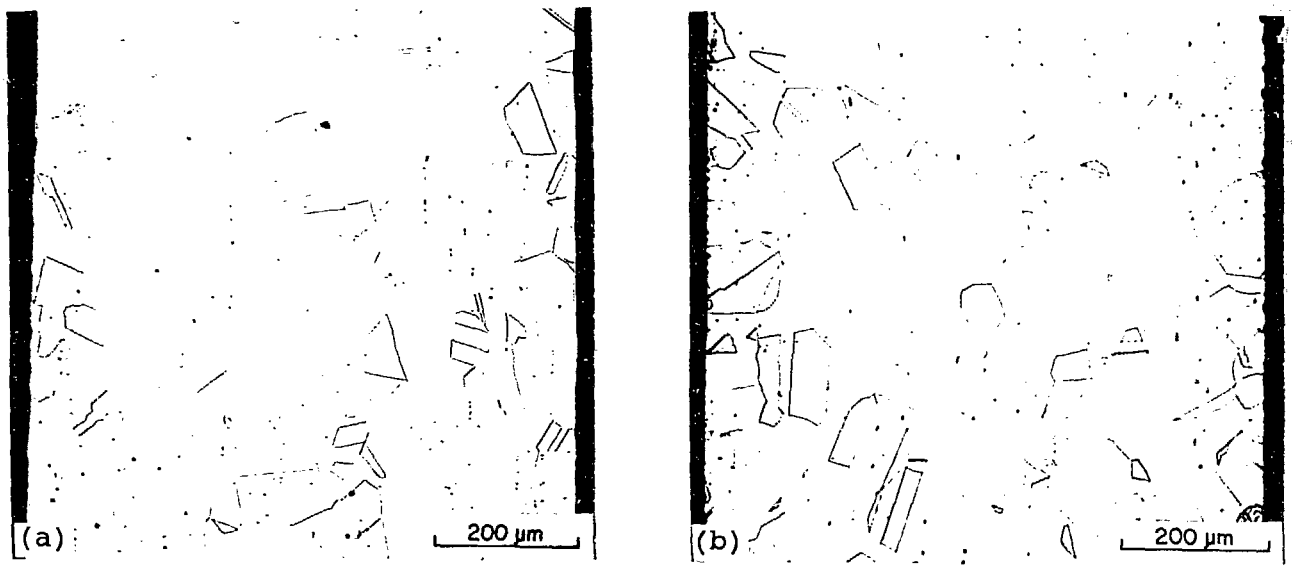

Fig. 7. Microstructures of (a) type 316 stainless steel and (b) an Fe-20%Mn-12%Cr-0.25%C alloy, both solution annealed 1 h at 1050°C.

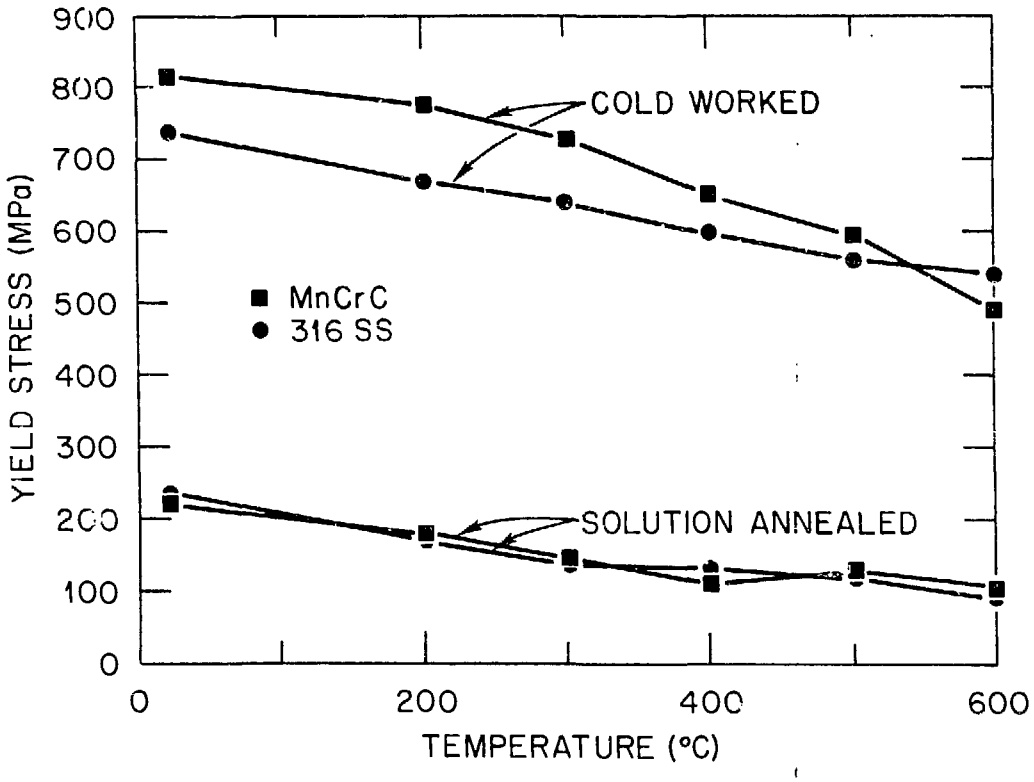

Fig. 8. Yield stress behavior as a function of test temperature of type 316 stainless steel and an Fe-20%Mn-12%Cr-0.25%C alloy (MnCrC) after solution annealing 1 h at 1050°C and after 20% cold work.

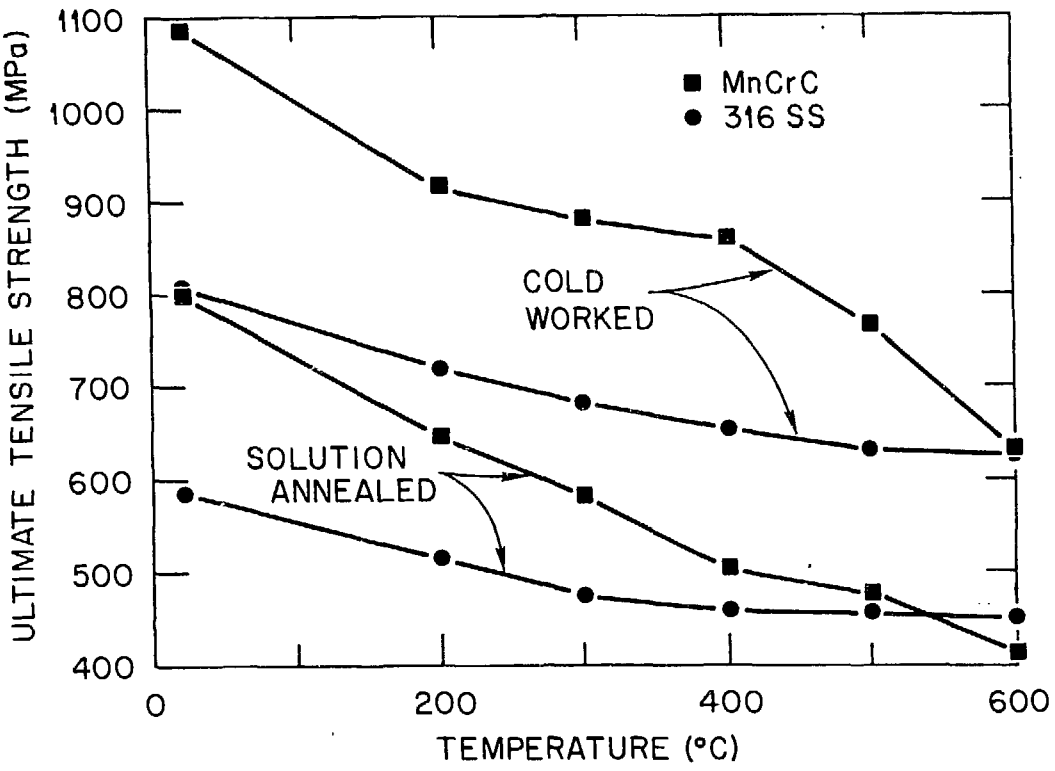

Fig. 9. Ultimate tensile strength behavior as a function of test temperature of type 316 stainless steel and an Fe-20%Mn-12%Cr-0.25%C alloy (MnCrC) after solution annealing 1 h at 1050°C and after 20% cold work.

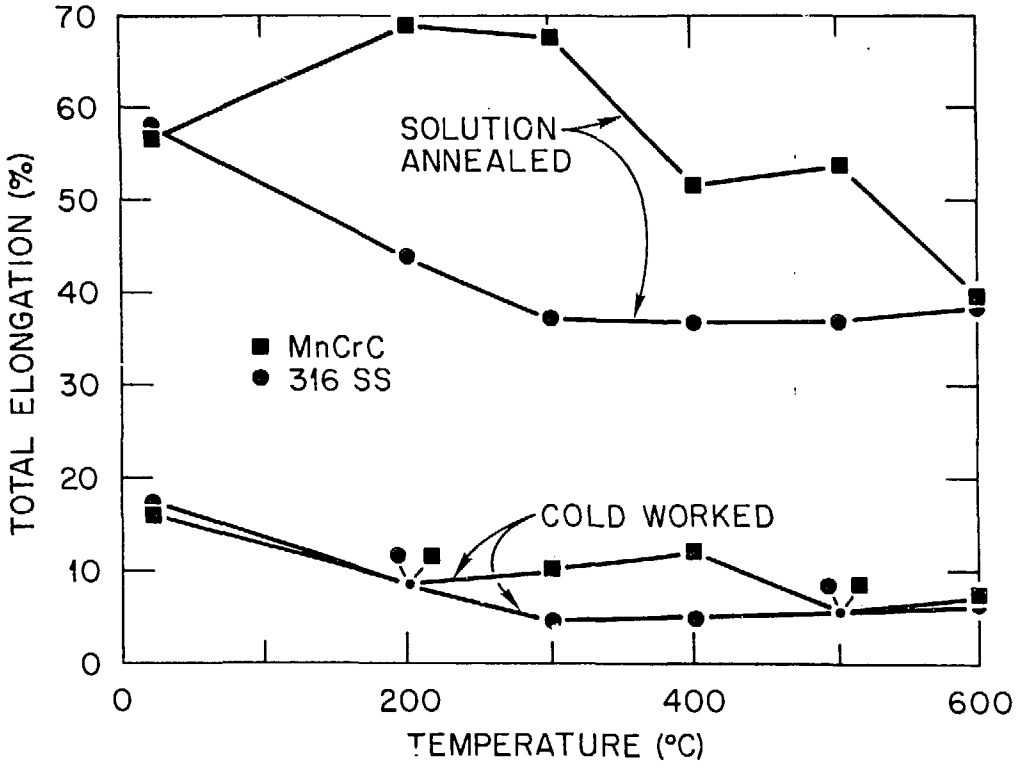

Fig. 10. Total elongation behavior as a function of test temperature of type 316 stainless steel and an Fe-20%Mn-12%Cr-0.25%C alloy (MnCrC) after solution annealing 1 h at 1050°C and after 20% cold work.

DISCLAIMER